



Enhancing flame and electrical surface discharge resistance in silicone rubber composite insulation through aluminium hydroxide, clay, and glass fibre additives

M. Tariq Nazir¹ · Arslan Khalid² · Cheng Wang² · Imrana Kabir² · Guan H. Yeoh² · B. Toan Phung³

Received: 24 November 2023 / Revised: 6 February 2024 / Accepted: 6 March 2024 / Published online: 15 March 2024
© The Author(s) 2024

Abstract

Silicone rubber (SR) is a leading polymer used in electrical outdoor insulation applications due to its superior hydrophobic characteristics. However, the low flame and electrical surface discharge resistance of SR limit its broad viability and challenge its integrity in severe outdoor working conditions. This work attempts to explore the flame retardancy and surface discharge characteristics of SR co-filled with aluminium hydroxide (ATH), nanoclay montmorillonite (MMT), and chopped glass fibre (GF). Results indicate that the incorporation of ATH/MMT/GF could assist in improving the fire and surface discharge resistance of the SR material. It is noted that the maximum average rate of heat emission (MARHE) and total smoke production (TSP) are measured at 24.93 kW/m² and 0.48 m² in SRE, relative to 61.29 kW/m² and 6.02 m² in SRB. Using finite element analysis (FEA), the maximum electric field strength is computed at 4.66 × 10⁶ V/m in the air gap coupled with a high-voltage (HV) plate and sample. SRE exhibits a higher partial discharge inception voltage (PDIV) value of 2.32 kV_{rms} than its counterparts, while the maximum discharge magnitude (Q_{max}) is computed at 7095 pC, relative to 7746 pC in SRB. SRE emerges as a preferable SR composite to be used in electrical insulation applications with excellent flame and surface discharge resistance characteristics.

Keywords Silicone rubber (SR) · Flame resistance · Discharge resistance · Electrical conductivity · Finite element analysis (FEA)

1 Introduction

Silicone rubber (SR) composite materials play a crucial role in electrical insulation applications, particularly in demanding outdoor environments [1, 2]. This is attributed to their exceptional surface hydrophobic nature, significantly enhancing their resistance against electrical arcing and discharges [3–5]. SR-based insulation offers multiple advantages, such as low weight, easy transportation, resistance

against vandalism, and excellent performance under highly polluted conditions [6–8]. Despite having several advantages, SR materials are flammable once they ignite, and this drawback limits their broad applicability in regions subjected to wildfire risks.

Intumescent additives are substantially employed by researchers to enhance the flame retardancy of polymeric materials [9–14]. Li et al. [15] successfully attached melamine (MEL) and phytate compounds to multi-walled carbon nanotubes (MWNCTs) and then incorporated them into the polyamide. It was reported that smoke release was impeded by 48%, and the limiting oxygen index (LOI) was enhanced to 26.4%. Zhao et al. [16] developed a magnesium-based curing agent as an intrinsic flame retardant for epoxy, using magnesium hydroxide (MDH), 9,10-dihydro-9-oxa-10-phosphaphenanthrene-10-oxide (DOPO), maleic acid, and ammonium polyphosphate (APP) compounds. It was exhibited that the LOI of epoxy was improved to 26% with the addition of 7% of intumescent additives, whereas the peak heat release rate (HRR), total heat release (THR),

✉ M. Tariq Nazir
tariq.nazir@rmit.edu.au

¹ School of Engineering, RMIT University, Melbourne, VIC 3000, Australia

² School of Mechanical and Manufacturing Engineering, University of New South Wales, Sydney, NSW 2052, Australia

³ School of Electrical Engineering and Telecommunications, University of New South Wales, Sydney, NSW 2052, Australia

smoke production rate (SPR), and total smoke production (TSP) were reduced by 54%, 35%, 43%, and 38%, respectively, as compared to pristine epoxy. Liu et al. [17] explored the flammability of polypropylene (PP) by using piperazine pyrophosphate (PAPP), and THR and peak HRR declined by 23% and 85%, respectively, relative to pristine PP. Ai et al. [18] investigated the flame resistance of a novel herbicide additive named amitrole modified through an organophosphorus compound incorporated into an epoxy polymer. It suggested that epoxy with only 7.5% content of flame retardant enhances the LOI of epoxy to 34%, and toxic gases emitted in the combustion process were impeded significantly. Zhu et al. [19] reported the fire retardancy of epoxy employing the P/N-containing oligomer and APP. LOI was improved to 30%, while peak HRR and TSP appeared with considerably lower values, relatively.

Non-intumescent and ceramifiable fire retardants were also developed to enhance the flame retardancy of polymers by generating a ceramic-like barrier against heat [20]. Anyszka et al. [21] explored the ceramisability of SR under fire using montmorillonite (MMT). SR created a compact, porous, and durable layer of ceramic, sticking MMT particles to the SR matrix with heat exposure. Lou et al. [22] investigated the flame retardancy of SR using APP, calcium carbonate, mica, and glass additives and reported that LOI increased to 31.2%, while peak HRR and THR were reduced compared to pristine SR. Hanu et al. [23] reported the thermal stability and fire retardancy of SR using iron oxide, glass, and mica additives. SR offered excellent thermal stability performance with the addition of 15% glass and mica powder, whereas SR showed a lower peak HRR by replacing the glass with iron oxide additives. Furthermore, Li et al. [24] explored the viability of glass and zinc borate, fumed silica, aluminium hydroxide (ATH) and MDH, calcium carbonate, and silicone oil in enhancing the flame characteristics of the SR matrix. Results showed that the LOI value increased to 34.8%, and flexural strength reached 9.70 MPa with the optimised addition of the above-mentioned fillers.

As far as the partial discharge (PD) resistance of electrically insulating material is concerned, Lee et al. [25] suggested that epoxy composites with micron and nano-sized silica offered better discharge resistance relative to their pristine form. Tanaka et al. [26] investigated the PD resistance of epoxy filled with modified clay particles, and results exhibited that micro/nano epoxy composites offered excellent resistance due to the impact of the interaction zone. Li et al. [27] studied the role of particle size on the discharge resistance and dielectric strength of epoxy. There was an obvious improvement seen in PD resistance with increasing micron particles, while nano-sized particles assisted slightly in enhancing the dielectric strength. Nazir et al. [28] found that the partial discharge inception voltage (PDIV) of EPDM polymer increased from 2.58 to 3.25 kV_{rms} as the doping

level of nano-boron (BN) powder rose from 0 to 7%, and there was a notable decrease in surface discharge parameters. Wang et al. [29] reported the thermal properties and PD resistance of SR using micron/nano BN powder. It exhibited that thermal conductivity and PDIV linearly increased with the increasing BN contents in the composites.

Literature suggests that intumescent fire retardants are excellent flame retardants but result in an increment in the electrical conduction capability of polymers due to the swelling and moisture absorption nature of additives [30, 31]. In addition, powders such as inorganic silica, alumina, and BN are excellent in providing adequate PD resistance to electrical insulation and thermal characteristics [7, 32] but lack in providing flame retardancy. Here, the authors have synthesised the SR co-filled composites by adopting the novel strategy of ATH/MMT/chopped glass fibre (GF) hybrid additives and explored the flame and surface discharge resistance of the co-filled composites to be used as industrial electrical insulating material.

2 Experimental

2.1 Materials

A pure form of liquid silicone (SYL-GARD™184) was received from DOW chemical in two parts ((A) base polymer and (B), curing agent) with a base viscosity of 5100 cP and density of 1.03 g/cm³. Moreover, the ATH (density = 2.42 g/cm³) is natural flame resistive and was procured from Redox, Australia with a mean grain size of 5 microns, while GF (E-glass) was purchased from Allnex, Australia, with a filament length of 6000 microns and an average diameter of 13 microns. MMT nanoclay (CLOSITE Na⁺, density = 2.86 g/cm³) is received from ResChem, Australia, with a mean size of 25 microns. Figure 1 exhibits the micron structure of all additives used in this work.

2.2 Composites' fabrication

A block diagram in Fig. 2 illustrates the process used for the fabrication of SR co-filled composites. The pertinent amount of all additives was weighed after drying at 110 °C for 12 h in an oven [33]. Initially, the required amount of SR part A was taken in a lab polyethylene cup. In the first stage, ATH particles were mixed with SR part A using a hand stirrer, followed by a sharp-blade mechanical mixer for 30 s. A similar process was repeated with the MMT and GF additives as per the required formulation. Later, the cross SR composites were reacted with part B of the matrix in a 10:1 ratio. The matrix was again mechanically mixed for 30 s with care to ensure that the composites were not heated up. Afterward, the composites were placed in a lab vacuum pump chamber

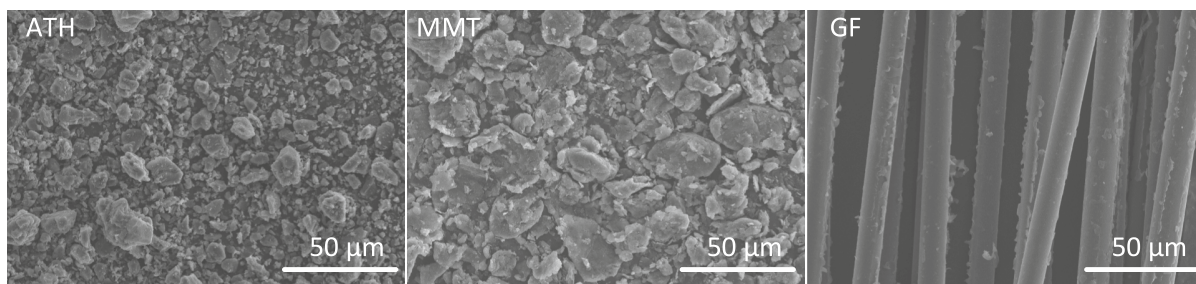


Fig. 1 SEM micrographs of additives used for the fabrication of co-filled SR composites

and degassed until no trapped air was seen on the top surface in the form of bubbles. The moulds were preheated in the oven to prevent the settling of additives on the surface of the moulds. Finally, the moulds were placed in the lab oven, and the curing was performed at 120 °C for 1800s. SR composites with five different formulations were prepared, as shown in Table 1. All specimens were thoroughly washed with ethanol and water, then dried in an oven at 80 °C for a couple of hours.

2.3 Characterisation

The microstructure of the SR composites was evaluated via SEM (Hitachi S3400, Mito, Japan). SEM was operated at an accelerated voltage level of 15.0 kV. Before SEM imaging, the specimen was sputter-painted with a fine coating of gold to achieve the required conductivity. Furthermore, a PerkinElmer-STA 6000 was engaged to analyse the chemical functional groups with the addition of the additives.

The thermal stability and degradation of the SR composite are evaluated via thermogravimetric analysis (TGA) using the TGA/STA6000 (PerkinElmer) instrument. All TGA tests were conducted in a compressed air environment from 50 until 800 °C with an increasing rate of 10 °C per minute. Moreover, the electrical bulk conductivity of the specimens was assessed at 20 °C using the Keithley resistivity test setup as per ASTM D257. Additionally, the surface hydrophobic characteristic is evaluated via static water contact angle using the DMS-200, Kyowa, Japan. The size of the droplet was controlled at ~4.5 μL for each reading.

A laboratory cone calorimeter (FFT iCone Classic, UK) was used to study the flame-resistive parameters of

the specimens. All the cone tests were conducted at a heat flux of 35.0 kW/m², and specimens with a height and width of 10 cm were used, while the thickness was controlled at 0.3 cm for each sample.

The electrical field enhancement was studied using the finite element analysis (FEA) tool of ANSYS Maxwell. PD is a flashover or partial breakdown of the electrically insulating material because of electrical field enhancement relative to insulation withstand capability [34, 35]. The partial surface discharge occurred across the surface of the insulation, and it was measured using the IEC 60270 [36]. A circuit used for the surface discharge measurement is illustrated in Fig. 3. Surface discharge was measured using the instrument OMICRON MPD 600 coupled with a 1.0-nF coupling capacitor (*C_b*) and a quadripole unit. The voltage was supplied from a step-up transformer with the low voltage side energised from 0.240 kV_{rms} via a variac [37]. The parallel plate electrode (high-voltage (HV) electrode, thickness = 10 mm; diameter = 70 mm, and ground electrode, thickness = 25 mm; diameter 125 mm) geometry was used for surface discharge experiments. Figure 3 shows the schematic of an electrical circuit and parallel plate electrode system used in this work.

3 Results and discussion

3.1 Characterisation of composites

Figure 4a illustrates the microstructure of SR composites captured through SEM. Results suggest that all the additives are mixed with a high degree of homogeneity. ATH

Fig. 2 A block diagram for the fabrication of SR co-filled composites

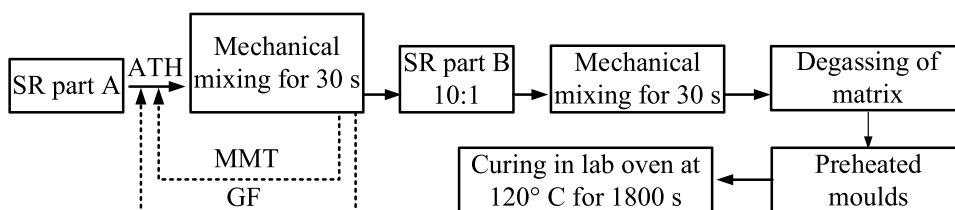


Table 1 A description of SR co-filled composites

Name	Matrix Part A (%)	Matrix part B (%)	ATH (%)	MMT (%)	GF (%)
SRA	90.90	9.10	0.0	0.0	0.0
SRB	63.60	6.40	30.0	0.0	0.0
SRC	58.20	6.80	30.0	5.0	0.0
SRD	60.90	6.10	30.0	0.0	3.0
SRE	56.40	5.60	30.0	5.0	3.0

and MMT particles are exhibited with non-uniform shapes, as seen in SRB and SRC. Interestingly, the GF additives are uniformly distributed in a 3D pattern, while ATH and MMT particles are observed in between and on the outer side of the threads penetrating the SR material. Moreover, Fig. 4b shows the critical functional groups found in the FTIR spectra of the SR matrix. The peaks found at 790 cm^{-1} , 1014 cm^{-1} , 1259 cm^{-1} , and 2960 cm^{-1} represent Si(CH₃)₂, Si-O-Si, Si-CH₃, and CH₃(C-H), respectively [7]. An interesting fact of the FTIR result is observed in the wavenumber range of 3250 cm^{-1} to 3700 cm^{-1} . No peak is observed in the pure SRA, but interestingly, a group of four identical peaks is seen in counterparts, as shown in Fig. 4c. These peaks represent the presence of hydroxyl functional groups in the moisture content of ATH particles.

Figure 4d shows the TGA profiles of the composites. The first degradation in filled composites is observed in the range of 219 to $380\text{ }^{\circ}\text{C}$, which could be due to the deterioration of ATH additives in this range, while the second dip in the range of 400 to $610\text{ }^{\circ}\text{C}$ shows the full depolymerisation of polymeric chains of the composites. Interestingly, SRA appears with a minor first deterioration dip, while it is found major in counterparts due to ATH decomposition. This is the reason that the starting decomposition temperature of the composites in the second stage is delayed in the filled SR composites. The initial decomposition temperature at the

second stage is measured at $398\text{ }^{\circ}\text{C}$, $428\text{ }^{\circ}\text{C}$, $435\text{ }^{\circ}\text{C}$, $432\text{ }^{\circ}\text{C}$, and $440\text{ }^{\circ}\text{C}$ in SRA, SRB, SRC, SRD, and SRE, respectively.

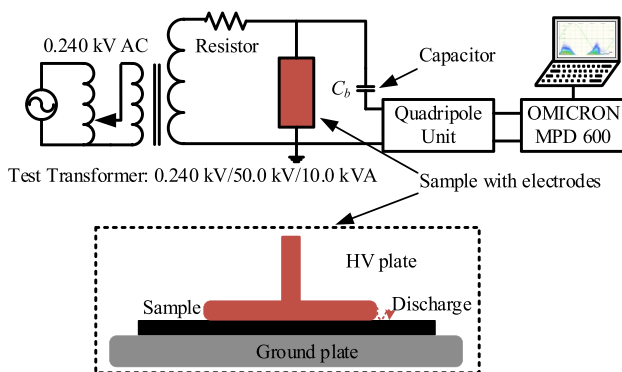
Figure 4e exhibits the electrical bulk conductivity of the SR specimens. The bulk conductivity of the SR composites is measured at $1.777 \times 10^{-11}\text{ S/cm}$, $1.434 \times 10^{-11}\text{ S/cm}$, $1.527 \times 10^{-11}\text{ S/cm}$, $1.596 \times 10^{-11}\text{ S/cm}$, and $1.808 \times 10^{-11}\text{ S/cm}$ for SRA, SRB, SRC, SRD, and SRE, respectively. It is found that ATH addition reduces the electrical conductivity of the composite, while it linearly increases with the addition of MMT and GF, as seen in SRC, SRD, and SRE.

The hydrophobic water contact angle of selected composites is shown in Fig. 4f. Hydrophobicity is a key surface property for high-voltage outdoor insulation, which renders excellent pollution flashover performance to SR insulation [38]. The contact angle is measured at 109.2° , 106° , 108.3° , 116.5° , and 115.5° in SRA, SRB, SRC, SRD, and SRE. The high hydrophobicity in the SRD and SRE composites could be due to the presence of GF, which may enhance the surface roughness of composites, and hence, it may increase the static water drop angle [39].

3.2 Cone calorimeter test

To understand the flame resistance of the SR co-filled composites, Fig. 5 illustrates the profiles of HRR, average rate of heat emission (ARHE), THR, SPR, TSP, and total oxygen consumed (TOC) produced from the cone calorimeter test. Table 2 shows the key data points extracted from the profiles. Results suggest that the peak HRR, maximum average rate of heat emission (MARHE), THR, peak SPR, TSP, and TOC are decreased with the addition of solely ATH, ATH/MMT, and ATH/GF in SR, as seen in SRB, SRC, and SRD. MMT and GF help in improving the fire resistance of composites in SRC and SRD, as MARHE and TSP reduce to 46.62 kW/m^2 and 1.49 m^2 in SRC and decline to 33.11 kW/m^2 and 1.03 m^2 in SRD, respectively, relative to both measured at 61.29 kW/m^2 and 6.02 m^2 in SRB. Moreover, it is evidenced that the presence of MMT/GF jointly with ATH in SRE can further aid in aggrandising the fire resistance of SR. Therefore, MARHE and TSP are computed at 24.93 kW/m^2 and 0.48 m^2 in SRE. A similar trend is also observed in the time to ignition (TI) and time to peak heat release (TP). The higher TI and TP of SRC, SRD, and SRE relative to SRB confirm the excellent fire retardancy of co-filled composites compared to SRB and SRA.

The excellent performance of composites in the cone calorimeter test could be attributed to the natural inherent flame retardancy characteristics of ATH and MMT. ATH is a natural compound with three hydrated water molecules present in its structure [40]. Upon decomposition, ATH releases its water vapours, reduces the combustion process of polymers, and results in the formation of char residue of

**Fig. 3** Schematic of surface discharge resistance measuring circuit

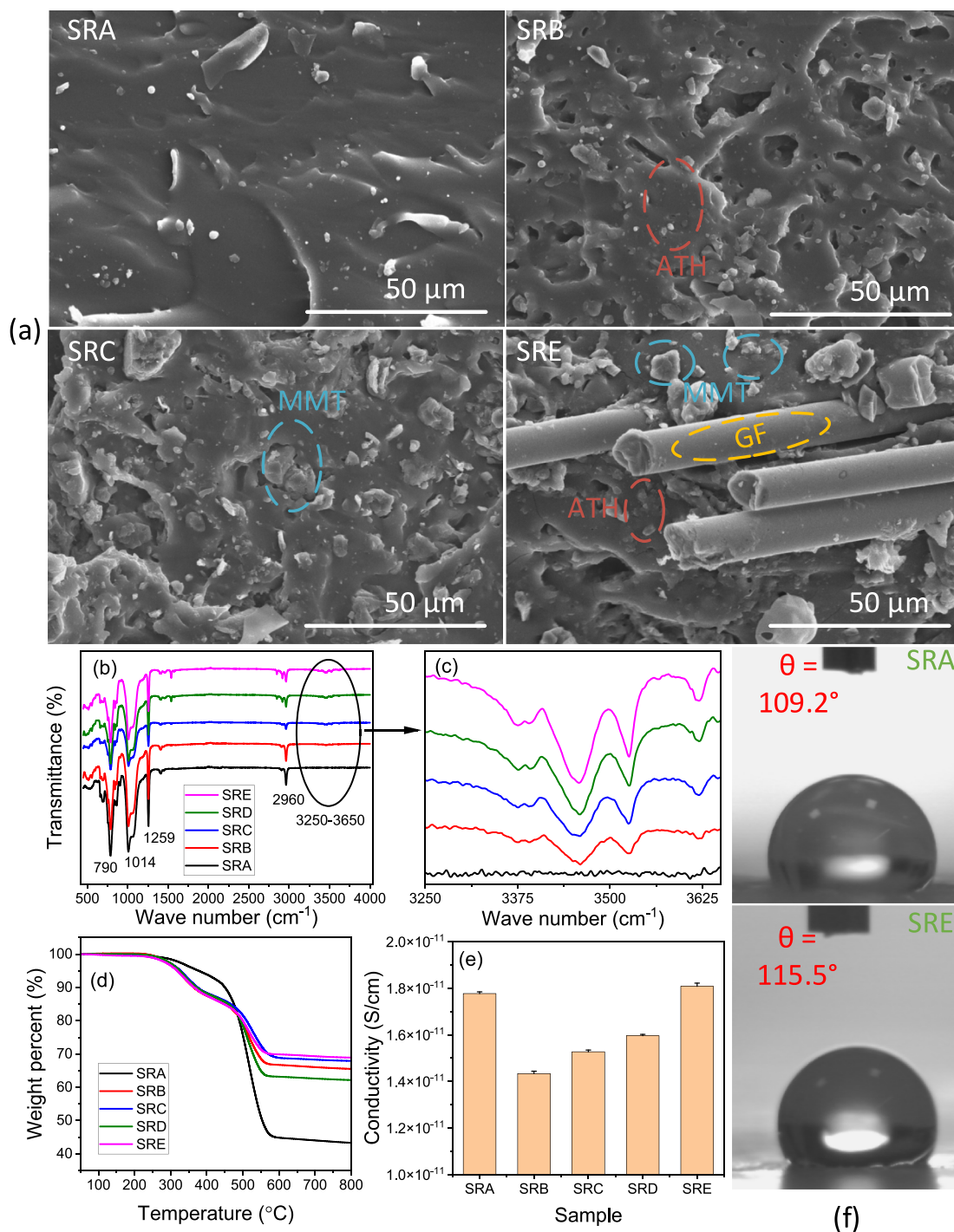


Fig. 4 Characterisation studies of SR co-filled composites **a** SEM microstructure of composites, **b** FTIR profiles of composites, **c** hydroxy functional groups in magnified FTIR profiles, **d** TGA stud-

ies, **e** bulk electrical conductivity of composites, and **f** static water contact angle of composites

aluminium oxide. MMT is a natural inorganic flame retardant for polymers without the production of toxic gases [41]. MMT decomposes after flame exposure and generates protonic catalytic sites, which help in creating a stronger interaction with the char residue [33]. Hence, it is highly likely

that ATH/MMT jointly form a compact char residue that acts as a heat barrier against combustible gases, resulting in better flame resistance.

To understand the flame resistance mechanism, an SEM study is conducted for the char residue of the composites,

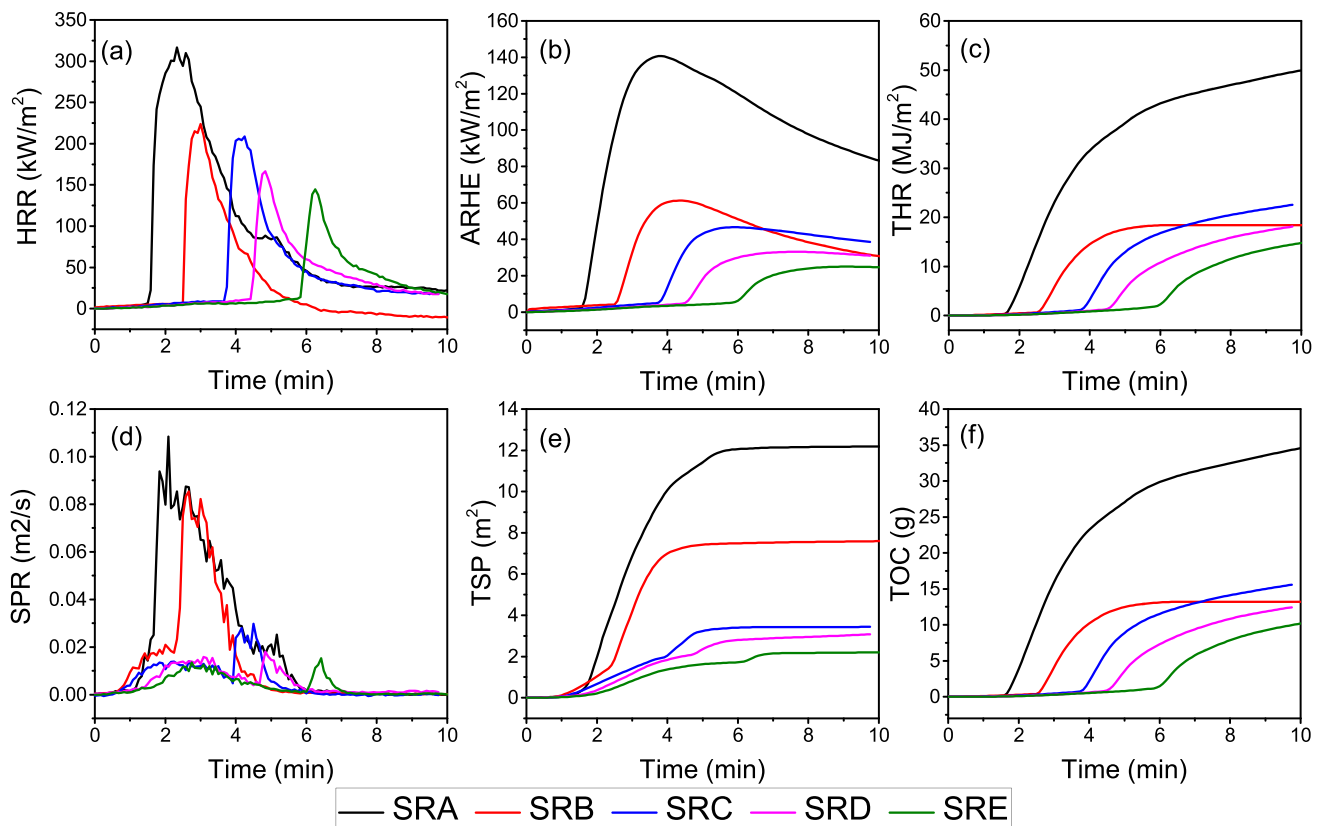


Fig. 5 Cone calorimeter data profiles of SR composites **a** HRR, **b** ARHE, **c** THR, **d** SPR, **e** TSP, and **f** TOC

as shown in Fig. 6. The char residue of SRA is observed as highly fluffy and fragile. Interestingly, the char residue of the filled composites is found solid, with a few weak points and cracks seen in SRB and SRC. Interestingly, the char residue of SRE is found compact and continuous relative to its counterparts; therefore, cone parameters are improved relatively. It is believed that GF is a non-flammable additive and acts as a fire barrier and reinforcing agent [42, 43]. Moreover, the SEM study of SRE confirms that GF assists in the formation of compact char, which is interlocked by the GF threads, and hence, it renders extraordinary protection to SRE against flame.

3.3 Electrical surface discharge

To explain the electrical surface resistance of SR composites, the net electric field enhancement is studied through FEA simulation. A three-dimensional parallel plate electrode with the sample is simulated in ANSYS Maxwell, as shown in Fig. 7a. Figure 7b shows the net electrical field enhancement on the surface of the sample on a logarithmic scale with an applied voltage of 5.0 kV. A significant field enhancement is observed at the triple junction point of the top electrode, sample surface, and air media. The maximum field strength is computed at 4.66×10^6 V/m.

Table 2 Cone calorimeter data of SR composites

Sample	Peak HRR (kW/m ²)	MARHE (kW/m ²)	THR (MJ/m ²)	Peak SPR (m ² /s)	TSP (m ²)	TOC (g)	TI (s)	TP (s)
SRA	316.44	140.69	49.32	0.108	11.48	34.22	105.0	140.0
SRB	223.76	61.29	17.82	0.085	6.02	12.83	148.0	180.0
SRC	208.55	46.62	21.02	0.030	1.49	14.61	234.0	255.0
SRD	166.49	33.11	16.41	0.018	1.03	11.35	277.0	290.0
SRE	144.63	24.93	12.49	0.015	0.48	8.68	361.0	375.0

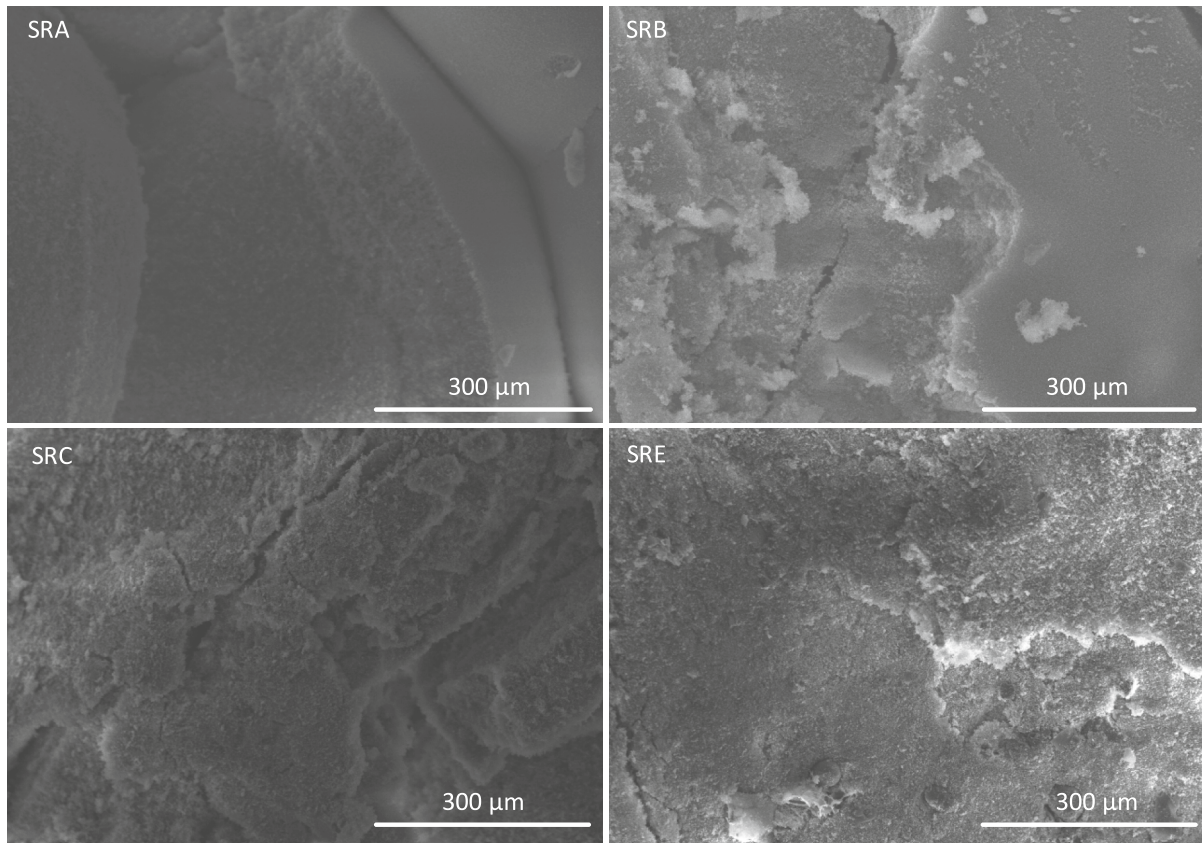


Fig. 6 Microstructure of char residue of SR composites

Moreover, the electric field is plotted across a line bisecting the sample fixed on the surface. Figure 8 illustrates the electric field strength on the surface of the sample along the line. It shows that there is no significant variation in the electric field with the

change in the permittivity of the SR composites. Furthermore, Fig. 8 confirms that there is a significant field enhancement in the air gap between the sample and the bottom electrode, leading to high ionisation and initiating partial surface discharge activity.

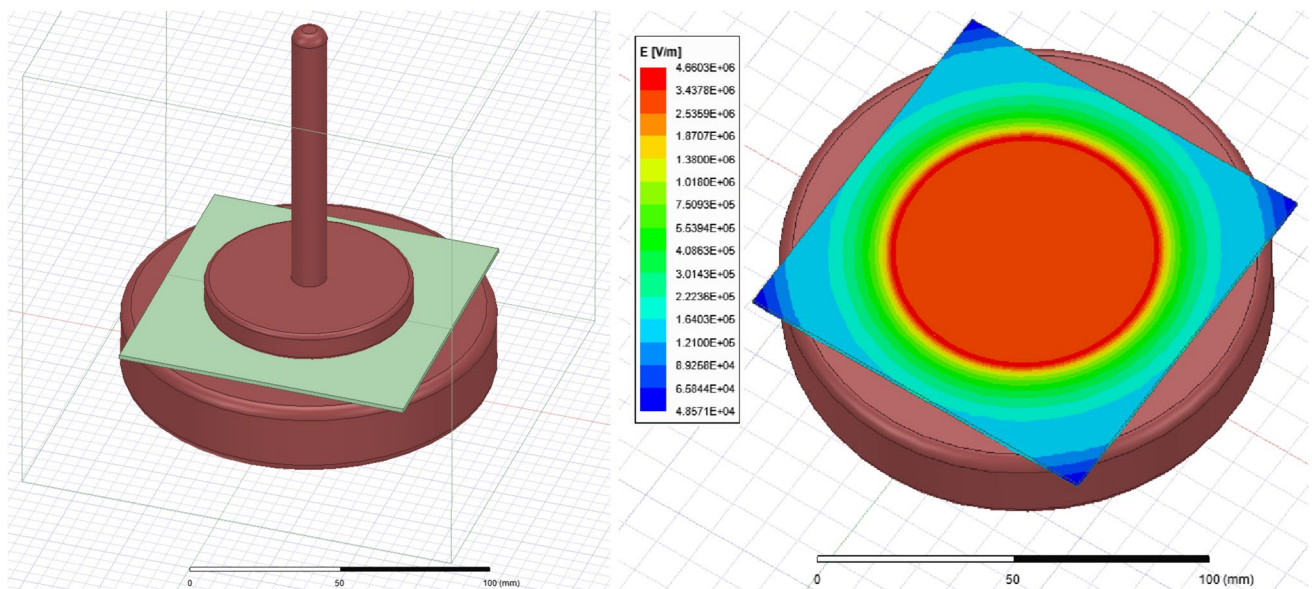


Fig. 7 FEA simulation study **a** ANSYS Maxwell 3D model and **b** electric field distribution on the surface of the sample

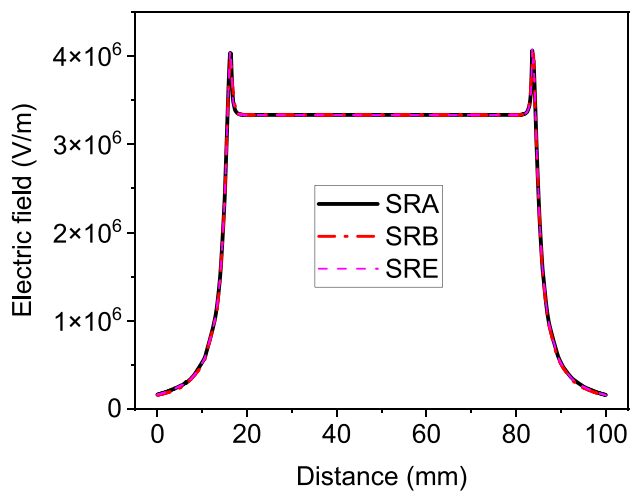


Fig. 8 A variation in the electric field across a line on the surface of the sample

For the surface discharge resistance study of SR composites, the partial discharge patterns are recorded at the PDIV of composites and a fixed voltage level of 5.0 kV_{rms}. PDIV is measured by ramping up the voltage for each sample until PD pulses are detected. For PDIV, the phase-resolved partial discharge pattern (PRPD) is recorded for 30 s with a threshold of 5 pC. Figure 9a and b show the

PRPD pattern of SRA and SRE at PDIV. Figure 9c and d show the PRPD patterns of SRA and SRE at a constant root mean square voltage of 5.0 kV recorded for 3 min with a threshold of 50 pC. PDIV and key electrical discharge parameters at 5.0 kV are extracted from the recorded PD data, as shown in Table 3.

Results show that the addition of particles in SR composites results in a reduction of PDIV relative to pristine SRA. PDIV of SRC, SRD, and SRE is measured at 1.48 kV_{rms}, 2.30 kV_{rms}, and 2.32 kV_{rms}, respectively, compared to 1.96 kV_{rms} in SRB. PDIV increases in SRD and SRE, indicating excellent electrical discharge resistance, while PDIV drops in SRC. This could be due to a significant increment in the capacitance, the permittivity of SRC with high dielectric loss, and reduced electrical dielectric strength [44].

At 5.0 kV, discharge parameters are analysed to further explore the discharge resistance of composites. As shown in Table 3, Q_{max} , $Q_{average}$, and repetition rate are computed at 7095 pC, 436 pC, and 31,919 pulses/s in SRE, respectively, compared to 7746 pC, 441 pC, and 43,187 pulses/s in SRB. The excellent surface discharge resistance of SRE with improved PDIV and lower surface discharge parameter values could be attributed to the excellent resistance provided by ATH/MMT/GF jointly embedded in SR [28, 45]. The co-filled additives act as a barrier against the movement of free electrical charges along the surface of

Fig. 9 Phase-resolved partial discharge pattern of composites **a** SRA at PDIV, **b** SRE at PDIV, **c** SRA at 5.0 kV, and **d** SRE at 5.0 kV

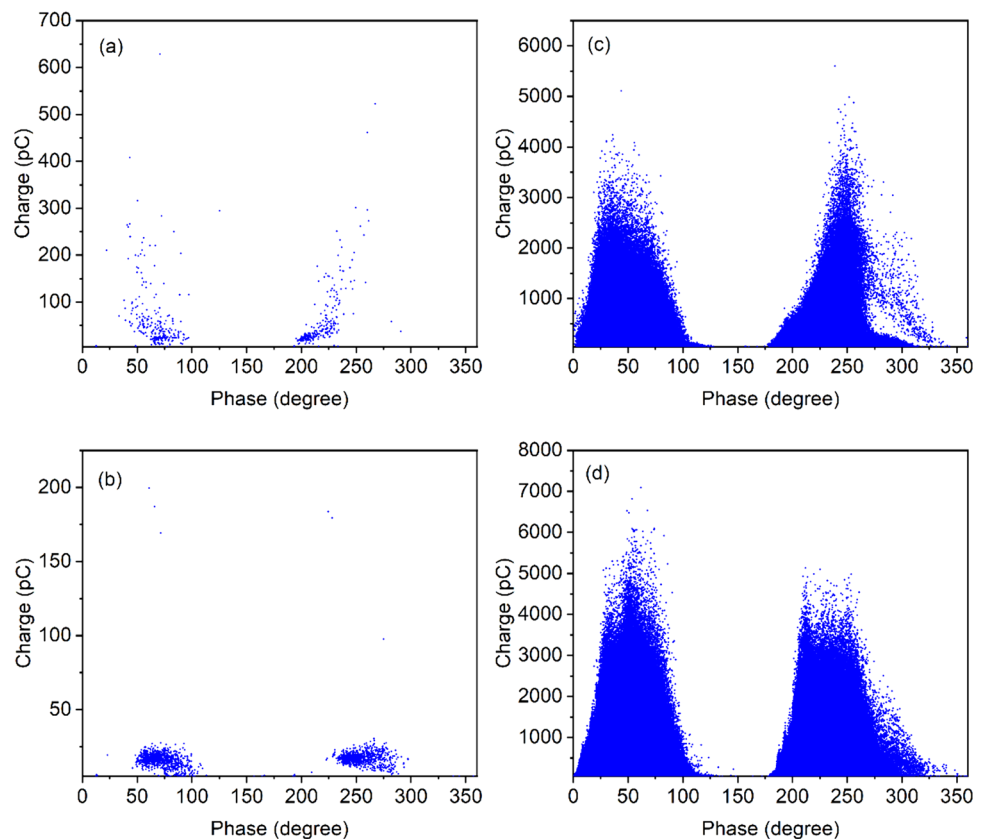


Table 3 Key surface discharge data of SR composites

Sample	PDIV (kV _{rms})	Surface discharge parameters at 5.0 kV _{rms}			
		Q_{\max} (pC)	Q_{average} (pC)	PD number	Repetition rate (pulses/s)
SRA	2.56	5599	304	1,753,872	9744
SRB	1.96	7746	441	6,153,663	34,187
SRC	1.48	14,679	476	7,220,011	40,111
SRD	2.30	8514	450	5,864,854	32,583
SRE	2.32	7095	436	5,745,447	31,919

the samples, which tends to increase the PDIV and reduce Q_{\max} , Q_{average} , and repetition rate.

4 Conclusion

This work addresses the fire resistance parameters, electrical field modelling, and electrical surface discharge resistance of SR matrix co-filled with ATH, MMT, and GF additives. It is concluded that ATH, ATH/MMT, and ATH/MMT/GF significantly increase the flame resistance of SR by decreasing the peak HRR, MARHE, THR, peak SPR, TSP, and TOC of the SR composites. SRE offers a 59% and 92% reduction in MARHE and TSP relative to SRB, respectively. A linear increment in TP and TI also validates the extraordinary resistance of composites against flame. It is also summarised that a significant electrical field enhancement is seen at the triple junction point of the top HV plate, sample, and air gap, which tends to start the surface discharge activity on the surface of the composites. Furthermore, it is concluded that the addition of the additives results in enhanced PDIV values, while there is a considerable reduction seen in the Q_{\max} , Q_{average} , and repetition rate of ATH/MMT/GF co-filled composites. SRE presents an 8%, 1%, and 7% reduction in Q_{\max} , Q_{average} , and repetition rate, respectively, relative to SRB. It is concluded that the addition of MMT and GF within the only ATH-filled SR could result in enhancing the flame and electrical surface discharge resistance of the SR material for use as industrial electrical insulating material.

Acknowledgements This work received financial support from RMIT University, Melbourne, through the Vice Chancellor's Postdoctoral Research Fellowship. We also acknowledge the partial discharge test facility provided by the HV laboratory of UNSW Sydney.

Author contribution The concept and design of the study were the result of the collaborative efforts of all authors. M. Tariq Nazir was responsible for experimentation, analysis, data curation, draft—writing, revision, funding acquisition, and resources. Arslan Khalid and Cheng Wang were responsible for characterisation and fire testing. Imrana Kabir contributed to the characterisation and revision of the manuscript. B. Toan Phung and Guan H. Yeoh provided resources and supervision.

Funding Open Access funding enabled and organized by CAUL and its Member Institutions This work received financial support from RMIT University, Melbourne, through the Vice Chancellor's Postdoctoral Research Fellowship.

Data availability The data that support the findings of this study are available from the corresponding author.

Declarations

Competing interests The authors declare no competing interests.

Open Access This article is licensed under a Creative Commons Attribution 4.0 International License, which permits use, sharing, adaptation, distribution and reproduction in any medium or format, as long as you give appropriate credit to the original author(s) and the source, provide a link to the Creative Commons licence, and indicate if changes were made. The images or other third party material in this article are included in the article's Creative Commons licence, unless indicated otherwise in a credit line to the material. If material is not included in the article's Creative Commons licence and your intended use is not permitted by statutory regulation or exceeds the permitted use, you will need to obtain permission directly from the copyright holder. To view a copy of this licence, visit <http://creativecommons.org/licenses/by/4.0/>.

References

1. Saleem MZ, Akbar M (2022) Review of the performance of high-voltage composite insulators. *Polymers* 14:431
2. Shit SC, Shah P (2013) A review on silicone rubber. *National academy science letters* 36:355–365
3. Reynders J, Jandrell I, Reynders S (1999) Review of aging and recovery of silicone rubber insulation for outdoor use. *IEEE Trans Dielectr Electr Insul* 6:620–631
4. Gubanski S, Dornfalk A, Andersson J, Hillborg H (2007) Diagnostic methods for outdoor polymeric insulators. *IEEE Trans Dielectr Electr Insul* 14:1065–1080
5. Ye J, Jin H, Zu Z, Yu B, Xiang H, Zhang M (2023) Dynamic crosslinked silicones and their composites: a review. *Eng Sci* 22:815
6. Amin M, Akbar M, Amin S (2007) Hydrophobicity of silicone rubber used for outdoor insulation (an overview). *Rev Adv Mater Sci* 16:10–26
7. Nazir MT, Phung B, Hoffman M (2016) Performance of silicone rubber composites with SiO₂ micro/nano-filler under AC corona discharge. *IEEE Trans Dielectr Electr Insul* 23:2804–2815

8. Vazirinasab E (2020) Superhydrophobic silicone-based nanocomposites for application to high voltage insulator: Université du Québec à Chicoutimi
9. Bar M, Alagirusamy R, Das A (2015) Flame retardant polymer composites. *Fibers and polymers* 16:705–717
10. Liu BW, Zhao HB, Wang YZ (2022) Advanced flame-retardant methods for polymeric materials. *Adv Mater* 34:2107905
11. Huang P, Wu F, Pang Y, Wu M, Lan X, Luo H et al (2019) Enhanced dispersion, flame retardancy and mechanical properties of polypropylene/intumescent flame retardant composites via supercritical CO₂ foaming followed by defoaming. *Compos Sci Technol* 171:282–290
12. Huang G, Wang S, Song Pa WuC, Chen S, Wang X (2014) Combination effect of carbon nanotubes with graphene on intumescent flame-retardant polypropylene nanocomposites. *Compos A: Appl Sci Manuf* 59:18–25
13. Kandola BK, Horrocks A, Myler P, Blair D (2002) The effect of intumescent on the burning behaviour of polyester-resin-containing composites. *Compos A Appl Sci Manuf* 33:805–817
14. Subasinghe A, Bhattacharyya D (2014) Performance of different intumescent ammonium polyphosphate flame retardants in PP/kenaf fibre composites. *Compos A Appl Sci Manuf* 65:91–99
15. Li Y, Wang J, Xue B, Wang S, Qi P, Sun J et al (2022) Enhancing the flame retardancy and UV resistance of polyamide 6 by introducing ternary supramolecular aggregates. *Chemosphere* 287:132100
16. Zhao P, Zeng W, Yang Z, Yang Y, Li J, Shi J et al (2021) Preparation of a novel functionalized magnesium-based curing agent as an intrinsic flame retardant for epoxy resin. *Chemosphere* 273:129658
17. Liu W, Ding L, Wang L, Zhang C, Yang W, Liu D et al (2023) A rational design of functionalized black phosphorus cooperates with piperazine pyrophosphate to significantly suppress the fire hazards of polypropylene. *Chemosphere* 314:137686
18. Ai Y-F, Liu X-D, Bai W-B, Lin Y-C, Xie R-R, Jian R-K (2022) From herbicide to flame retardant: the lamellar-like phosphorus-bridged amitrole toward high fire safety epoxy resin with light smoke and low toxicity. *Chemosphere* 291:132704
19. Zhu Z-M, Wang L-X, Dong L-P (2019) Influence of a novel P/N-containing oligomer on flame retardancy and thermal degradation of intumescent flame-retardant epoxy resin. *Polym Degrad Stab* 162:129–137
20. Li Y-M, Hu S-L, Wang D-Y (2020) Polymer-based ceramifiable composites for flame retardant applications: a review. *Compos Commun* 21:100405
21. Anyszka R, Bieliński D, Pędzich Z, Szumera M (2015) Influence of surface-modified montmorillonites on properties of silicone rubber-based ceramizable composites. *J Therm Anal Calorim* 119:111–121
22. Lou F, Yan W, Guo W, Wei T, Li Q (2017) Preparation and properties of ceramifiable flame-retarded silicone rubber composites. *J Therm Anal Calorim* 130:813–821
23. Hanu LG, Simon GP, Cheng Y-B (2006) Thermal stability and flammability of silicone polymer composites. *Polym Degrad Stab* 91:1373–1379
24. Li Z, Liang W, Shan Y, Wang X, Yang K, Cui Y (2020) Study of flame-retarded silicone rubber with ceramifiable property. *Fire Mater* 44:487–496
25. Lee C-H, Park J-J (2010) The partial discharge resistances of epoxy-nano-and-micro composites. *Trans Electr Electron Mater* 11:89–91
26. Tanaka T, Ohki Y, Ochi M, Harada M, Imai T (2008) Enhanced partial discharge resistance of epoxy/clay nanocomposite prepared by newly developed organic modification and solubilization methods. *IEEE Trans Dielectr Electr Insul* 15:81–89
27. Li Z, Okamoto K, Ohki Y, Tanaka T (2011) The role of nano and micro particles on partial discharge and breakdown strength in epoxy composites. *IEEE Trans Dielectr Electr Insul* 18:675–681
28. Nazir MT, Phung B, Sahoo A, Yu S, Zhang Y, Li S (2019) Surface discharge behaviours, dielectric and mechanical properties of EPDM based nanocomposites containing nano-BN. *Appl Nanosci* 9:1981–1989
29. Wang Y, Wu J, Yin Y, Han T (2020) Effect of micro and nano-size boron nitride and silicon carbide on thermal properties and partial discharge resistance of silicone elastomer composite. *IEEE Trans Dielectr Electr Insul* 27:377–385
30. Wang Q, Chen Y, Liu Y, Yin H, Aelmans N, Kierkels R (2004) Performance of an intumescent-flame-retardant master batch synthesized by twin-screw reactive extrusion: effect of the polypropylene carrier resin. *Polym Int* 53:439–448
31. Nazir MT, Khalid A, Akram S, Mishra P, Kabir II, Yeoh GH et al (2023) Electrical tracking, erosion and flammability resistance of high voltage outdoor composite insulation: research, innovation and future outlook. *Mater Sci Eng R Rep* 156:100757
32. Han H, Sun H, Lei F, Huang J, Lyu S, Wu B et al (2021) Flexible ethylene-vinyl acetate copolymer/fluorographene composite films with excellent thermal conductive and electrical insulation properties for thermal management. *ES Mater Manuf* 15:53–64
33. Nazir MT, Khalid A, Wang C, Akram S, Li Y, Wong K et al (2022) Fire and electrically resistive silicone elastomer/alumina trihydrate composites derived from nanoclay and chopped glass fibres for industrial fire safety. *Process Saf Environ Prot* 167:257–261
34. Saman NM, Zakaria IH, Ahmad MH, Abdul-Malek Z (2021) Effects of plasma treated alumina nanoparticles on breakdown strength, partial discharge resistance, and thermophysical properties of mineral oil-based nanofluids. *Materials* 14:3610
35. Wang M, Du B, Kong X, Li Z, Han T, Ma Y (2022) Effects of high magnetic field on partial discharge and dielectric breakdown behavior of silicone rubber. *IEEE Trans Dielectr Electr Insul* 29:915–923
36. Standard I (2000) High-voltage test techniques: partial discharge measurements. IEC-60270 13–31
37. Nazir MT (2018) Study on degradation of polymeric nanocomposite dielectric materials used for high voltage outdoor insulation: UNSW Sydney
38. Khan H, Mahmood A, Ullah I, Amin M, Nazir MT (2021) Hydrophobic, dielectric and water immersion performance of 9000 h multi-stresses aged silicone rubber composites for high voltage outdoor insulation. *Eng Fail Anal* 122:105223
39. Nazir MT, Wang C, Phung B, Wong K, Yeoh G (2022) Enhanced fire retardancy with excellent electrical breakdown voltage, mechanical and hydrophobicity of silicone rubber/aluminium trihydroxide composites by milled glass fibres and graphene nanoplatelets. *Surf Interfaces* 35:102494
40. Han Z, Wang Y, Dong W, Wang P (2014) Enhanced fire retardancy of polyethylene/alumina trihydrate composites by graphene nanoplatelets. *Mater Lett* 128:275–278
41. Zhang G, Wang J (2018) Preparation of novel flame-retardant organoclay and its application to natural rubber composites. *J Phys Chem Solids* 115:137–147
42. Shao H, Wang T, Zhang Q (2010) Ceramifying fire-resistant polyethylene composites. *Adv Compos Lett* 19:096369351001900501
43. Kamath G, Mishra B, Tiwari S, Bhardwaj A, Marar SS, Soni S et al (2022) Experimental and statistical evaluation of drilling induced damages in glass fiber reinforced polymer composites—Taguchi integrated supervised machine learning approach. *Eng Sci* 19:312–318
44. Nazir MT, Khalid A, Wang C, Yeoh G, Phung B, Akram S et al (2023) Flame resistive silicone elastomeric powder-based coatings with excellent localized dielectric breakdown strength, loss tangent and thermal stability for electrical insulation. *Powder Technol* 416:118184

45. Kozako M, Fuse N, Ohki Y, Okamoto T, Tanaka T (2004) Surface degradation of polyamide nanocomposites caused by partial discharges using IEC (b) electrodes. *IEEE Trans Dielectr Electr Insul* 11:833–839

Publisher's Note Springer Nature remains neutral with regard to jurisdictional claims in published maps and institutional affiliations.